Proceedings of the 9th U.S. National and 10th Canadian Conference on Earthquake Engineering
Compte Rendu de la 9ième Conférence Nationale Américaine et
10ième Conférence Canadienne de Génie Parasismique
July 25-29, 2010, Toronto, Ontario, Canada • Paper No 319

VARIABLE-FREQUENCY ROCKING BEARING FOR NEAR-FAULT SEISMIC ISOLATION

Lyan-Ywan Lu[1], Tzu-Ying Lee[2], I-Ling Yeh[3], Hsun Chang[3], Shih-Wei Yeh[3]

ABSTRACT

Because a base isolated structure is usually a long-period dynamic system, an excessive response can be easily induced by a near-fault earthquake that possesses a long-period pulse-like waveform. To alleviate this problem, a rocking bearing that has a variable isolation frequency is proposed in this study. The proposed rocking bearing has an articular (ball-and-socket) joint on the top and a rocking surface with a variable curvature on the lower part. The articular joint is connected to the super-structure through a mounting plate. In an earthquake, the rocking surface of the bearing will rock back-and-forth on a base plate that is mounted on the ground or the foundation of the structure. By properly selecting the bearing's geometric parameters, the isolation stiffness of the proposed rocking bearing can be a function of the bearing displacement. As a result, the bearing's isolation frequency becomes variable and can be determined by the geometric parameters, exclusively. In this study, the bearing's rocking surface is defined by a six-order polynomial function, so the restoring force of the bearing exhibits a softening behavior followed by a hardening behavior. This mechanical behavior aims to suppress the maximum structural acceleration and isolator displacement, simultaneously. By comparing with the response of a conventional FPS isolation system, the isolation performance of the rocking bearing with its rocking surface defined by the six-order polynomial is investigated numerically in this study.

Introduction

A typical seismic isolation system usually has a flexible layer to uncouple the ground motion from the super-structure. In order to reduce the residual base displacement of the isolated structure after an earthquake, the flexible layer must incorporate a resilient mechanism. The resilient mechanism will produce the isolation stiffness, which is usually designed much lower than the super-structural stiffness. As a result, a structure isolated by a conventional seismic isolation system is usually a long-period structural system with a constant isolation frequency. It has been shown that conventional isolation systems can be very effective in mitigating the seismic responses of structures subjected to regular earthquakes (Naeim and Kelly 1999). Nevertheless, recent studies have also revealed that a conventional isolation system may induce an excessive isolator

[1] Professor, Dept. of Construction Engineering, National Kaohsiung First Univ. of Sci. & Tech., Kaohsiung, Taiwan
[2] Assistant professor, Department of Civil Engineering, National Central University, Taoyuan County, Taiwan.
[3] Graduate Research Assistant, National Kaohsiung First Univ. of Sci. & Tech., Kaohsiung, Taiwan

displacement in a near-fault earthquake that contains a long-period pulse wave component (Jangid and Kelly 2001, Lu et. al. 2002). This long-period pulse component, whose pulse period can range from 1.4 to 7 seconds, can be very detrimental to low-frequency structural systems, such as a base isolated structure (Hall 1995).

In order to reduce the excessive isolator displacement induced by a near-fault earthquake, in this paper, a variable-frequency rocking bearing called a polynomial rocking bearing (PRB) is proposed. Since the rocking surface of the PRB is defined by a six-order polynomial, the isolation frequency provided by the PRB becomes a function of the isolator displacement, rather than a constant. The feasibility and isolation performance of the PRB will be investigated in this paper by using a numerical method.

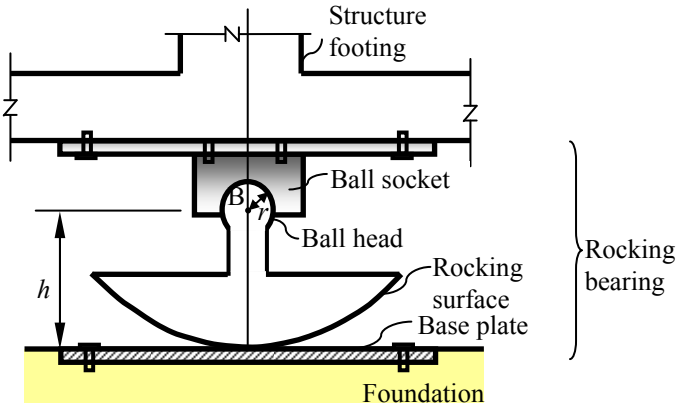

Figure 1. The variable-frequency rocking bearing installed under a structure footing.

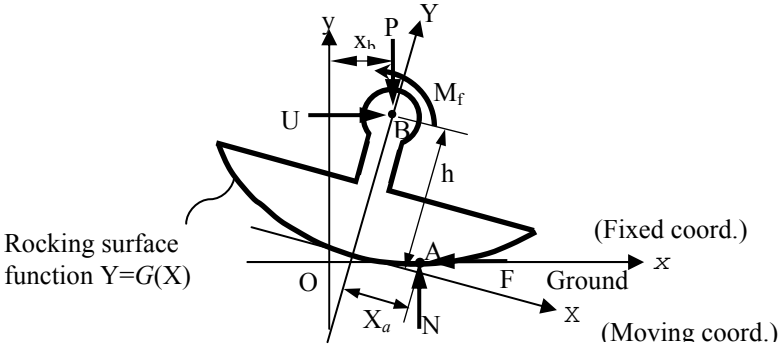

Figure 2. Free body diagram of the rocking bearing.

Theory of Variable-Frequency Rocking Bearing

Configuration of the rocking bearing

Fig. 1 shows the proposed rocking bearing installed under the structure footing. As shown in the figure, the rocking bearing has an articular (ball-and-socket) joint on the top and a rocking surface with a base plate on the lower part. The articular joint is connected to the super-structure through a mounting plate, while the base plate is mounted on the ground or the foundation of the structure. In an earthquake, the rocking surface of the bearing will rock back-and-forth on the base plate, thus the transmitted ground motion onto the super-structure can be mitigated. The rocking surface, which is usually axially symmetric, must be concaved and may have a variable curvature.

Restoring force of the rocking bearing

The mechanical behaviour of an isolator usually can be characterized by its force-displacement relation. Here, the force and displacement mean the isolator horizontal shear and the isolator displacement, respectively. In this subsection, a formula describing the force-displacement relation for a rocking bearing with variable frequency will be given. Fig. 2 shows the free-body-diagram of the rocking bearing. In Fig. 2, there are two coordinate systems: *x*-*y* and X-Y coordinates. The *x*-*y* system is a fixed coordinates, while the X-Y system is a moving coordinates that is attached to the bearing and will rock along with the bearing. Also shown in Fig. 2, the rocking bearing has two major design parameters: the bearing height *h* and the geometric function *G*(X) of the rocking surface. For the convenience, the function *G*(X) is usually expressed in terms of the X-Y coordinates, i.e., Y=*G*(X).

In Fig. 2, there are four forces and one moment M_f applying on the bearing. These forces or moment are defined as follows: *P* is the vertical load; *N* is the normal force applied on the contact point A of the rocking surface; *F* is the friction force applied on point A; *U* denotes the horizontal shear force that interacts between the bearing and the super-structure; M_f represents the moment caused by friction in the articular joint. Note that the shear *U* is equivalent to the horizontal seismic force transmitted to the isolated structure. The shear *U* of the rocking bearing can be derived by taking the moment equilibrium equation about the contact point A. The derived total shear U can be written in the following form

$$U = u_r + u_f \tag{1}$$

The terms u_r and u_f in Eq. 1 represent the restoring force and the friction force components in the total shear *U*, respectively. u_f is contributed by the friction moment M_f in the bearing, while u_r depends on the geometry of the bearing's rocking surface. The detail derivation of u_r and u_f were given in the reference (Lu et. al. 2009). While the derived u_f will be discussed later, the restoring force u_r can be written explicitly as

$$u_r = P\bar{u}_r, \text{ where } \bar{u}_r = \left[\frac{-\left(h - G(\mathrm{X}_a)\right)G'(\mathrm{X}_a) + \mathrm{X}_a}{h - G(\mathrm{X}_a) + \mathrm{X}_a\, G'(\mathrm{X}_a)}\right] \tag{2}$$

In the above equations, X_a is the X-coordinate of the contact point A in X-Y coordinate system (see Fig. 2), and $G'(\mathrm{X})$ denotes the first derivative of *G*(X) about variable X. Note that in Eq. 2 $\bar{u}_r$ represents the normalized restoring force with respect to the bearing's vertical load *P*, since $\bar{u}_r = u_r / P$. Eq. 2 demonstrates that the restoring force u_r of the rocking bearing is a function of X_a, *G*(X) and *h*, and is proportional to the vertical load *P*. Note that as shown in Fig. 2, X_a is not the base displacement of the superstructure. The base displacement (or isolator displacement) should be defined as the horizontal displacement x_b of point B in Fig. 2. Point B is the center of the articular joint. Furthermore, because the horizontal displacement of point B is equal to the *x*-coordinate of point B in the *x*-*y* coordinate system, it can be derived that

$$x_b = \frac{\left(h - G(\mathrm{X}_a)\right)G'(\mathrm{X}_a) - \mathrm{X}_a}{\sqrt{1 + G'(\mathrm{X}_a)^2}} + \int_0^{\mathrm{X}_a} \sqrt{1 + G'(\mathrm{X})^2}\, d\mathrm{X} \tag{3}$$

Investigating Eq. 2 and 3, one should realize that it is difficult to directly express the restoring force u_r as an explicit function of the isolator displacement x_b. However, the relationship

between u_r and x_b does exist and can be established through the intermediate variable X_a. A numerical tool is generally required, when the relation curve of u_r and x_b is to be depicted.

Equivalent horizontal friction force of the rocking bearing

As mentioned previously, the friction moment M_f in the articular joint of the bearing causes the equivalent horizontal friction component u_f shown in Eq. 1. At any time instant, the magnitude of u_f will rely on the current status of the bearing motion, which has two motion states, i.e., rocking and stick (non-rocking) state. In the rocking state, the magnitude of u_f will be equal to its maximum value denoted by $u_{f,\max}$, while in the stick state, u_f will be determined by the dynamic response of the isolated structure and its magnitude should not be greater than $u_{f,\max}$. u_f can be expressed as

$$\left|u_f\right| < u_{f,\max} \text{ (for stick state)} \tag{4.a}$$

$$\left|u_f\right| = u_{f,\max} \text{ (for rocking state)} \tag{4.b}$$

where

$$u_{f,\max} = \frac{r\sqrt{1+G'(\mathrm{X}_a)^2}}{h - G(\mathrm{X}_a) + \mathrm{X}_a G'(\mathrm{X}_a)}\mu P \tag{5}$$

where μ represent the material friction coefficient between the ball head and ball socket of the articular joint, and r denotes the radius of the ball head (see Fig. 1). Eq. 5 has shown that the maximum friction force $u_{f,\max}$ is also a function of X_a-coordinate. The complete derivation of Eq. 5 is given in the reference (Lu et. al. 2009).

Tangential isolation stiffness and isolation frequency

The tangential restoring stiffness k_r (or called instantaneous stiffness), which is defined as the rate of change of the restoring force, of the proposed bearing can be computed by taking the derivative of u_r with respect to the base displacement x_b, i.e.,

$$k_r(\mathrm{X}_a) = \frac{du_r}{dx_b} = \frac{du_r(\mathrm{X}_a)/d\mathrm{X}_a}{dx_b(\mathrm{X}_a)/d\mathrm{X}_a} = \frac{P\bar{u}_r'(\mathrm{X}_a)}{x_b'(\mathrm{X}_a)} \tag{6}$$

In the last equation, u_r defined in Eq. 2 has been applied. Eq. 6 implies that the isolation stiffness is not a constant but a function of the base displacement x_b, since $\mathrm{X}_a = \mathrm{X}_a(x_b)$. Furthermore, by using Eq. 6, the tangential isolation frequency ω_b of the isolated structure can be computed by the following equation

$$\omega_b(\mathrm{X}_a) = \sqrt{\frac{k_r(\mathrm{X}_a)}{M}} = \sqrt{\frac{P\bar{u}_r'(\mathrm{X}_a)}{M\,x_b'(\mathrm{X}_a)}} \tag{7}$$

where M is the mass of the isolated super-structure. Notably, in Eq. 7 it is assumed that the super-structure behaves like a rigid body. Moreover, provided that the vertical load P, which is due to the structural weight, can be expressed as $P = M\,g$, one may use this equation in Eq. 7 and obtains

$$\omega_b(\mathrm{X}_a) = \sqrt{\frac{g\,\bar{u}_r'(\mathrm{X}_a)}{x_b'(\mathrm{X}_a)}} \tag{8}$$

From Eq. 8, it is evident that isolation frequency of the bearing is not a constant, but is an implicit function of the base displacement x_b and the geometric function $G(\mathrm{X})$, since $\bar{u}_r'$ is a function of $G(\mathrm{X})$ (see Eq. 2). It is for this reason that the proposed bearing is called the variable-frequency rocking bearing. Eq. 8 also demonstrates that the isolation frequency of the PRB is completely independent from the structural mass M. The variation of the isolation frequency gives the adaptability of the isolated system. By properly selecting the geometric function $G(\mathrm{X})$ of the sliding surface, the isolated system may possess favourable dynamic characteristics in different base displacement.

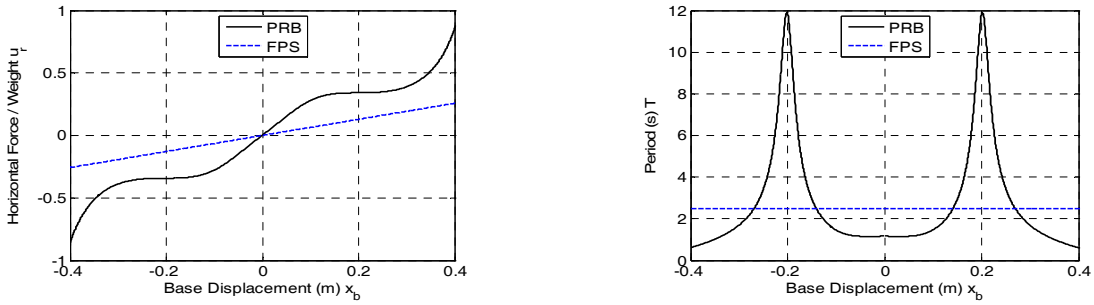

(a) Normalized restoring force (b) Isolation period

Figure 3. Comparison of FPS and PRB mechanical properties.

Polynomial Rocking Bearing (PRB)

In order to improve the isolation performance in near-fault earthquakes, in this study, the following sixth-order polynomial function has been chosen to define the geometry function $G(\mathrm{X})$ of the bearing's rocking surface:

$$G(\mathrm{X}) = c_1\mathrm{X}^6 + c_2\mathrm{X}^4 + c_3\mathrm{X}^2 \tag{9}$$

where c_1, c_2 and c_3 are three constant polynomial coefficients. Because the bearing's shape is defined by the above polynomial, it is called a *Polynomial Rocking Bearing* (PRB) in this study. By properly choosing the values of the three polynomial coefficients c_1, c_2 and c_3, the restoring-force function u_r of the PRB can possess a desired feature.

When the values of the height h and the coefficients c_1, c_2 and c_3 of the PRB are as given in Table 1, Fig. 3 shows the normalized restoring force $\bar{u}_r$ and the isolation period T_b $(=2\pi/\omega_b)$ of the PRB as a function of the base displacement x_b. In addition, for the purpose of comparison, the restoring force and isolation period of the friction pendulum system (FPS) isolator, whose parameter values are given in Table 1, are also depicted in Fig. 3. The FPS isolation system is a very commonly used sliding isolation system (Mokha 1991). As shown in Fig. 3(a), the PRB with the chosen coefficient values has a softening section followed by a hardening section, when the base displacement x_b increases. The isolation stiffness of the PRB is decreased in the softening section, while in the hardening section the stiffness is increased.

The purpose of the softening section is to mitigate the acceleration response in a smaller base displacement; while the purpose of the hardening section is to suppress the base displacement for a sever earthquake for the safety reason. In brief, the softening and hardening sections aim to control the structural acceleration and base displacement, respectively. Moreover, if $G(\mathrm{X})$ is substituted from Eq. 9 in Eq. 2 and 5, one is able to express the restoring force u_r and the maximum friction $u_{f,\max}$ of the PRB in terms of the polynomial coefficients c_1, c_2 and c_3.

Table 1. Parameters of PRB and FPS isolators used in numerical simulation.

PRB Parameter		Value	FPS parameter	Value
Equivalent horizontal initial friction coefficient μ_0		0.1	Sliding friction coefficient μ_{FPS}	0.1
Polynomial coefficient of rocking surface	c_1	30 (1/m^5)	Isolation period T_{FPS}	2.5s
	c_2	0.027 (1/m^3)		
	c_3	1.145 (1/m)	Isolation frequency ω_{FPS}	0.4Hz
Bearing height h		0.25 m		
Radius of ball head r		0.044 m		

Table 2. Superstructures parameters used in simulation.

Parameter	Value	Parameter	Value
Structure mass (m_s)	300 ton	Damping ratio (ζ_s)	5 %
Base mass (m_b)	100 ton	Stiffness (k_s)	3.289×10^4 kN/m
Natural frequency (ω_s)	1.67 Hz	Damping coeff. (c_s)	314 kN-s/m

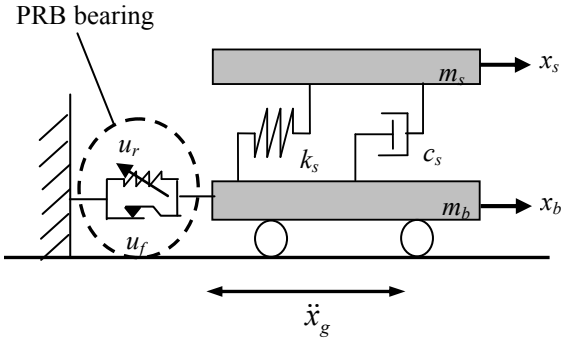

Figure 4. Mathematical model for a structure isolated by the PRB

Harmonic Steady-state Responses of Polynomial Rocking Bearing (PRB)

Mathematic model and numerical method

In following section, the performance of a structure isolated by the PRB and subjected to ground accelerations with near-fault characteristics will be evaluated by a numerical method. Fig. 4 shows the mathematical model of a structure isolated by the PRB bearings. To simplify the problem, the super-structure in Fig. 4 is modelled as a single-DOF system, so the study can focus on the PRB isolation performance. in Fig. 4, the symbols x_s and x_b denotes the relative-to-the ground displacements of the base and super-structure, while m_s and m_b represent the corresponding mass. In addition, as shown in Fig. 4, the friction force u_f and the resorting force u_r of the PRB is modelled by a friction element and a nonlinear spring, respectively. The equation of dynamics for the model of Fig. 4 can be written in a state-space form:

$$\dot{\mathbf{z}}(t) = \mathbf{A}\,\mathbf{z}(t) + \mathbf{B}(u_r(t) + u_f(t)) + \mathbf{E}\,\ddot{x}_g(t) \tag{10}$$

where $\mathbf{A}$ denotes the system matrix; $\mathbf{z}(t) = \{\dot{x}_s, \dot{x}_b, x_s, x_b\}^T$ is the state variables; $\ddot{x}_g(t)$ represents the ground acceleration; $\mathbf{B}$ is the isolator distribution matrix; $\mathbf{E}$ is the excitation distribution matrix. Note that in Eq. 10 both nonlinear terms $u_r(t)$ and $u_f(t)$ have been moved to

the right-hand side of the equation. In order to deal with these nonlinear forces more efficiently, in this study a numerical procedure developed based on the discrete-time state-space formulation and the shear-force balanced method (Lu et. al, 2006) was adopted for the analysis of the PRB isolated structure.

To be used in the numerical study of this paper, Table 2 lists the parametric values of the isolated structure, while Table 1 lists the parametric values of the PRB bearing. In addition, Table 1 also lists a FPS whose dynamic responses will be used for comparison purpose. Table 1 shows that the initial friction coefficient μ_0 of the PRB is chosen to be the same as the friction coefficient μ of the FPS. Table 2 also shows that the isolated structure has a natural frequency of 1.67 Hz representing a low-rise building.

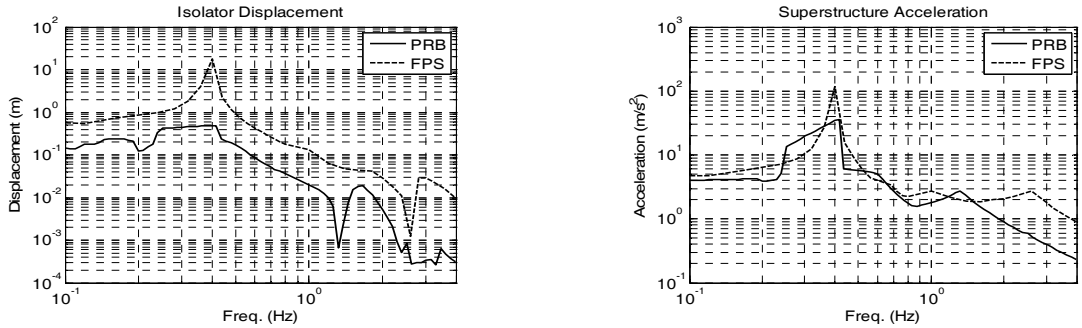

(a) Base displacement (b) Structural acceleration

Figure 5. Amplitudes of PRB and FPS harmonic steady-state responses (PGA = 0.4g)

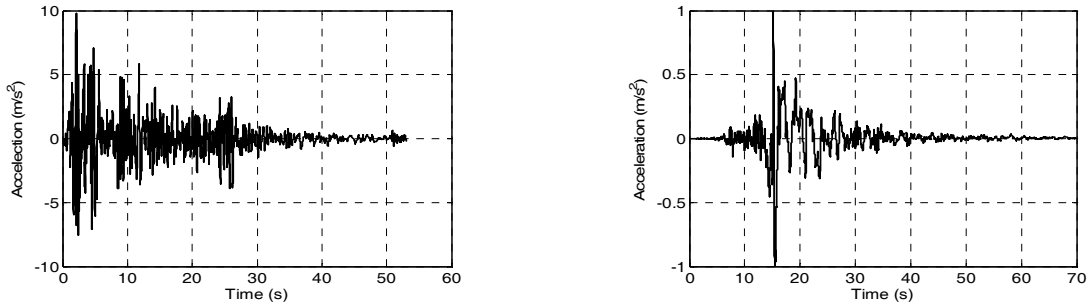

(a) El Centro (far-field) earthquake (b) Chi-Chi TCU068 (near-fault) earthquake

Figure 6. Ground accelerations used in simulation (PGA = 1g).

Comparison of harmonic responses of PRB and FPS

In order to investigate the dynamic behavior of the PRB under different excitation frequencies, a harmonic ground acceleration $\ddot{x}_g(t) = 0.4g\sin\omega_g t$ (where ω_g denotes the excitation frequency) is imposed to the isolated system in this subsection. Based on the simulated results, Fig. 5 compare the amplitudes of the steady-state responses of the PRB and the FPS isolation systems, as a function of the excitation frequency ω_g. Several observations can be made from Fig. 5: (1) In Fig. 5(a), as expected, a significant resonant response is occurred in the base displacement of the FPS at the isolation frequency around 0.4 Hz. On the other hand, no obvious resonant response is observed for the base displacement of the PRB system. This implies that the base displacement of the PRB will not be amplified by a low-frequency ground excitation. (2) In Fig. 5(b), the resonance of structural acceleration due to the vibration mode of the super-structure at 1.67 Hz has been mitigated in both PRB and FPS isolation cases. However, for the FPS, the resonance of structural acceleration still occurs around the isolation frequency of

0.4 Hz. On the other hand, for the PRB, Fig. 5(b) demonstrates the acceleration resonant response of the PRB is mitigated, although its acceleration response has a higher value in the frequency range between 0.2-0.5 Hz than in other frequency range.

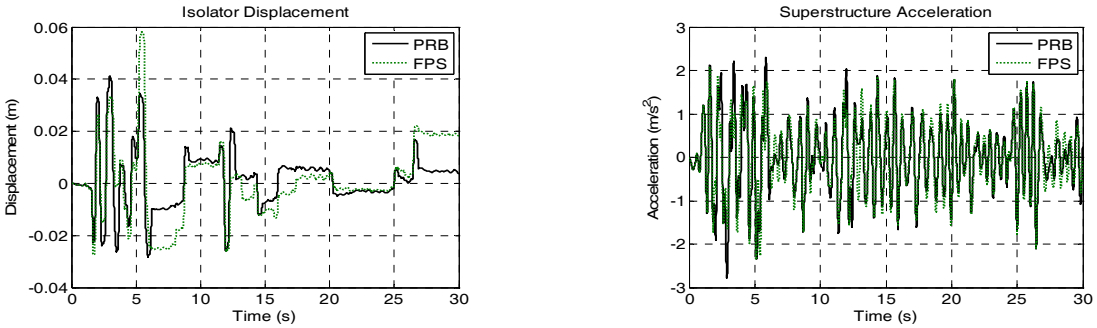

(a) Base displacement (b) Structural acceleration

Figure 7. Comparison of FPS and PRB responses for El Centro Earthquake (far-field, PGA = 0.4g)

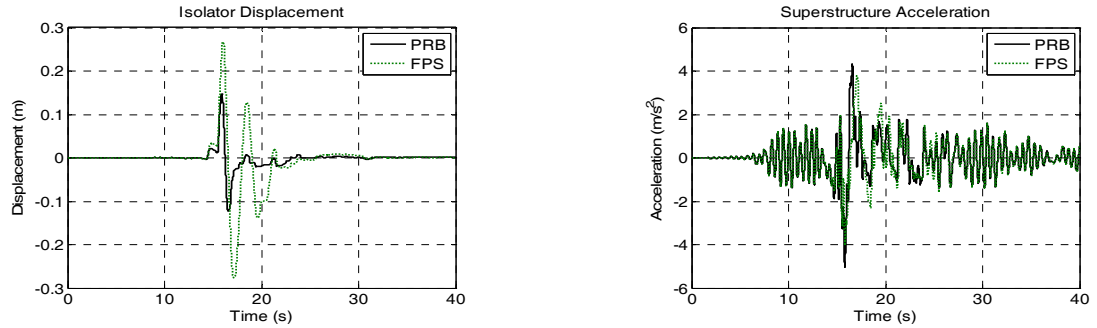

(a) Base displacement (b) Super-structural acceleration

Figure 8. Compare FPS and PRB responses for Chi-Chi TCU068 Earthquake (near-fault, PGA = 0.4g)

Seismic Performance of Polynomial Rocking Bearing

Comparison of FPS and PRB time history responses

In this section, two acceleration records measured from real earthquakes will be used as the input ground excitations in the numerical study. The detailed information about these two earthquakes is given below: (1) the El Centro (S00E) Earthquake, 18 May 1940, peak acceleration 0.341g. (2) Chi-Chi earthquake, station TCU068, 21 September 1999, peak acceleration 0.497g. The El Centro earthquake is a famous earthquake record that has been widely used in many seismic engineering studies. The Chi-Chi earthquake record was recorded by station TCU068 that is near a seismic fault. The waveforms of these two earthquakes are shown in Fig. 6. As shown in Fig. 6(b), long-period pulse-like waveforms can be clearly observed in the Chi-Chi (TCU068) earthquake. Therefore, in this study the Chi-Chi (TCU068) and El Centro earthquake are used to represent a near-fault and a far-field earthquake, respectively.

Fig. 7 compares the time history responses of the PRB and FPS isolation systems under the El Centro (far-field) earthquake, while Fig. 8 compares the responses due to the Chi-Chi (near-fault) earthquake. Note that the PGA (peak ground acceleration) of both ground motions has been scaled to 0.4g. From these two diagrams, it can be observed that as compared with the FPS response, the PRB effectively reduces the maximum base displacement, although its structural acceleration is slightly higher than that of the FPS. In particular, Fig. 8(a) shows that

the base displacement of the PRB is only about 50% of the FPS displacement. Moreover, Fig. 8(a) also demonstrates that FPS exhibits more obvious oscillation in the base displacement response, which is exerted by the long-period pulse component in the Chi-Chi earthquake.

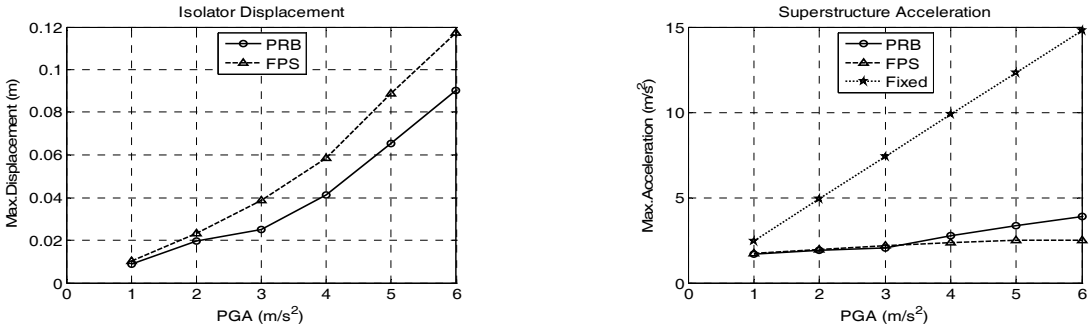

(a) Max. base displacement (b) Max. structural acceleration

Figure 9. Peak responses of PRB and FPS for different PGA levels (El Centro earthquake, far-field).

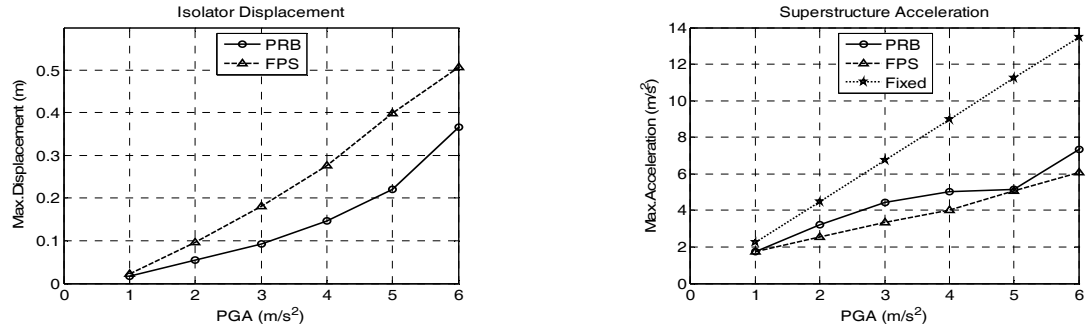

(a) Max. base displacement (b) Max. structural acceleration

Figure 10. Peak responses of PRB and FPS for different PGA levels (Chi-Chi earthquake, near-fault).

Comparison of PRB and FPS peak responses at different PGA levels

Because earthquake intensity is usually unpredictable, it would be beneficial to investigate how the PRB performs in an earthquake with different intensities. When the PGA is increased from 0.1 to 0.6g, Fig. 9 and 10 compare the peak responses of the PRB and FPS for the El Centro (far-field) and Chi-Chi (near-fault) earthquake, respectively. The peak acceleration response of an un-isolated (fixed-base) structure is also plotted in Fig. 9 and 10. From these two figures, the following observations can be made: (1) Fig. 9(a) and 10(a) show that in either the far-field or near-fault earthquake, the PRB is able to effectively reduce the base displacement of the isolation system, regardless the PGA level. However, comparing Fig. 9(a) and 10(a) reveals that the PRB is particularly effective in suppressing the base displacement induced by the near-fault earthquake. (2) When compared to the response of the fixed-base structure, Fig. 9(b) and 10(b) demonstrate that both the PRB and FPS are able to very effectively mitigate the peak structural acceleration. For the El Centro (far-field) earthquake with the PGA = 0.6g, the acceleration reduction rate for both the PRB and FPS can reach about 80%, while the reduction rate is about 50% for the Chi-Chi (near-fault) earthquake with the PGA = 0.6g. (3) When the comparison of the acceleration response is made between the PRB and FPS, Fig. 9(b) shows that for the far-field earthquake, the PRB and FPS have the same peak acceleration level for a PGA below 0.4g, but the PRB induces a slightly higher acceleration response when the PGA level becomes larger. On the other hand, Fig. 10(b) shows that for the near-fault earthquake, the PRB induces slightly higher acceleration response in most of the PGA range.

Conclusions

In order to improve the seismic isolation performance for earthquakes with near-fault characteristics, a variable-frequency rocking bearing called polynomial rocking bearing (PRB) is proposed in this study. Since the rocking surface of the PRB is defied by a polynomial function, the isolation stiffness and frequency of the PRB system become functions of the isolator displacement. The formula that describes the force-displacement relation and isolation frequency of the PRB were given in this study. Shown by the formula, the variable isolation frequency of the PRB is independent from the weight of the isolated structure and can be designed by properly choosing its geometric parameters. When the rocking surface of the PRB is defined by a six-order polynomial function, the restoring force of a PRB bearing will have a softening behavior followed by a hardening behavior, which aim to suppress the peak structural acceleration and peak base displacement, respectively. The result of numerical simulation has demonstrated that due to the feature of variable frequency, the proposed bearing is able to effectively mitigate the resonance effect induced by a low-frequency excitation. The result also shows that as compared to the FPS response, the PRB is particularly effective in suppressing the base displacement induced by a near-fault earthquake with a long-period pulse, although the structural acceleration response may be increased slightly. A comprehensive parametric study may be conducted for the PRB in the future, so the structural acceleration response of the PRB can be further improved.

Acknowledgement

This research was sponsored in part by the National Science Council of R.O.C. (Taiwan), through Grant 96-2622-E-327-011-CC3. This support is gratefully acknowledged.

References

Hall, J. F., T. H. Heaton, M. W. Halling, and D. J. Wald, 1995. Near-source ground motions and its effects on flexible buildings, *Earthquake Spectra* 11, 569-605.

Jangid, R. S., and J. M. Kelly, 2001. Base isolation for near-fault motion, *Earthquake Engineering and Structural Dynamics* 30, 691-707.

Lu, L. Y., M. H. Shih, C. S. Chang Chien, and W. N. Chang, 2002. Seismic performance of sliding isolated structures in near-fault areas, *Proceedings of the 7th US National Conference on Earthquake Engineering*, July 21-25, Boston, MA, USA.; Session AT-2.

Lu L. Y., L. L. Chung, L. Y. Wu, G. L. Lin, 2006. Dynamic analysis of structures with friction devices using discrete-time state-space formulation, *Computers and Structures,* 84(15-16), 1049-1071.

Lu, L. Y., T. Z. Lee, I. L. Yeh, H. Chang, 2009. Rocking Bearings with Variable Frequency for Near-fault Seismic Isolation (in Chinese), *Journal of the Chinese Institute of Civil and Hydraulic Engineering*, under review, submitted in February.

Mokha, A., M. C. Constantinous, A. M. Reinhorn, and V. A. Zayas, 1991. Experimental study of friction-pendulum isolation system, *Journal of Structural Engineering, ASCE* 117(4), 1201-1217.

Naeim, F. and J. M. Kelly, 1999. *Design of Seismic Isolated Structures: from theory to practice*, John Wiley & Sons.